Boosted Top Quark Tagging and Polarization Measurement using Machine Learning

Soham Bhattacharya,* Monoranjan Guchait,† and Aravind H. Vijay[‡]
Department of High Energy Physics, Tata Institute of Fundamental Research, Mumbai, India.

(Dated: July 9, 2022)

Machine learning techniques are used to explore the performance of boosted top quark tagging treating jets as images. Tagging performances are studied in both hadronic and leptonic channels employing convolutional neutral networks (CNN) based analysis along with boosted decision trees (BDT). It is observed that overall tagging performance in leptonic channel is better than the case of hadronic. This computer vision approach is also applied to distinguish the left and right polarized top quarks, and a measurable event asymmetry is constructed to estimate the polarization. Results indicates that the CNN based classifier is more sensitive than the standard kinematic variables to top quark polarization. It is observed that, overall tagging performance in leptonic channel is better than the case of hadronic and also serves as a better probe to study polarization.

INTRODUCTION: In the Standard Model (SM) of particle physics top quark plays an important role by its own virtue. For instance, how the larger mass of the top quark offered by the SM Higgs sector - is one of the most important and fundamental question in electroweak symmetry breaking. Moreover, in several of the BSM signal process, it is envisaged that the heavier non SM particles produced at a TeV energy get the access of the phase space, and may decay to a pair of very energetic top quark. The decay products from those boosted top quarks are so collimated that they form a single 'fat' jet, instead of multiple jets. Hence, it is very crucial to develop a strategy to tag boosted objects as a single fat jet preserving all properties of its origin [1, 2].

Already several techniques are available to tag boosted top jets which are widely used in searches of new physics models consisting very massive ($\sim \mathcal{O}(1~\text{TeV})$) particles [3–6]. While tagging the top jet in its hadronic channel is found to be more popular and well studied, but interest in tagging it in its leptonic channel is also growing. Meanwhile, efforts are in place to develop techniques to tag boosted top jets in its leptonic decay channel [7]. Needless to say, that more dedicated studies are needed to tag boosted leptonic top jet with more improved techniques.

Furthermore, another important aspect of top quark physics is its polarization measurement, potentially which can serve as an alternative avenue to probe the nature of BSM physics coupled with the top quark sector. It is well known that the kinematic properties, in particular angular distributions of top quark decay products are guided by its polarization which is essentially decided by the structure of couplings [8]. In previous studies lepton is found to be suitable object to study polarization of not so energetic top quark [9]. However, such methods are not effective in case of boosted top quark, because of the

overlapping of its decay products in the phase space [3–6]. Recently, strategies for the measuring the polarization of boosted top quark in its hadronic decay channel are proposed in Ref. [6] for the LHC experiments.

In recent times, a great deal of interest evolves to use the machine learning (ML) techniques involving deep neural network (NN) in analyzing physics events, and as well as data of LHC experiments [10]. Interestingly, the use of ML techniques have proven to be very powerful in improving the signal significance through better classification of signal and backgrounds, where cut based analysis is found to be less effective [10]. The key feature of this analysis is to represent jets as a set of data, namely jet image [11] which essentially a presentation of energy or transverse momentum (p_T) of its constituents in a plane transverse to the jet axis and divided it into $N \times N$ cells, called pixels. Low level object's information (e.g raw data, four momentum of jet constituents etc.) are used instead of high level objects to form those jet images. Energy or momentum deposited in each pixels, defined as the pixel strength resembling calorimeter cells, are used as inputs to train NN, and subsequently use that knowledge for testing to classify objects [12]. Among several existing NN used in High energy physics, the convolutional neural network (CNN) is widely used in classifying jets at the LHC and also used in this current analysis.

The primary focus of this analysis is two folds. In the first step, boosted top quark tagging performances are studied for both hadronic and leptonic channel using jet images as inputs to the CNN. Further, the classification performances are improved by using the CNN output as one of the inputs to BDT. Revisiting hadronic top tagging performances, we emphasize more on leptonic case, which we believe to the best of our knowledge not studied well using ML tools. In the second step, we investigate the performance of CNN in differentiating the left and right polarized boosted top quark for both hadronic and leptonic channels. Finally, a polarization sensitive event asymmetry variable is constructed to measure the polarization of boosted top quark. In general, it is found that the overall performances of leptonic channel of top quark

^{*} soham.bhattacharva@cern.ch

 $^{^{\}dagger}$ guchait@tifr.res.in

[‡] aravindhv10@gmail.com

is better than the hadronic case for both tagging and polarization measurements at the LHC.

METHODOLOGY: Boosted top quarks are produced by generating top pair $(pp \to t\bar{t})$ and $W'(pp \to t\bar{t})$ $W' \to tb$) events, where the W' mass is 3 TeV. Here on we refer them as $t\bar{t}$ and W' event samples, respectively. Light flavor jets produced in hard QCD events are treated as a background for boosted top jets. For our polarization study, left (right) polarized top quarks are produced from the aforementioned W' decay by setting the coupling strength $g_R = 0$ ($g_L = 0$) appearing in the W' decay vertex $\sim f_i \gamma^{\mu} [g_R(1+\gamma_5)+g_L(1-\gamma_5)]W'_{\mu}f_j$ [13]. In addition, top squark pair events $(pp \to \tilde{t}_1 \tilde{t}_1)$ are also generated, where the top squark of mass 1 TeV is forced to decay to a top quark and the lightest neutralino $(\tilde{\chi}_1^0)$ of mass 100 GeV. The chirality of this top quark can be controlled by appropriately adjusting the \tilde{t}_1 -t- $\tilde{\chi}_1^0$ coupling [6], setting the neutralino composition to be gaugino or Higgsino like. We refer to this as the SUSY sample henceforth. The $t\bar{t}$ and QCD samples are generated using PYTHIA8 [14]. In order to access the boosted region of the phase space, a hard cut of 400 GeV is applied to the traverse momenta (p_T) of the outgoing partons at tree-level. The W' sample is produced interfacing FeynRules v2.0 [15] in the framework of an effective theory with MadGraph5_aMC@NLO [16]. The SUSY sample is also generated using MadGraph5_aMC@NLO. Every sample is hadronized using PYTHIA8, with full multiparton interactions turned on. Finally, the detector simulation for each sample is performed using DELPHES v3.4 [17] with its Compact Muon Solenoid (CMS) card.

Fatjets of radii R=1.5 are reconstructed with the anti- k_T [18, 19] jet algorithm. A fatjet is categorized as a hadronic (leptonic) top jet if the jet axis lies within a cone of $\Delta R=\sqrt{\Delta y^2+\Delta\phi^2}<1.0$ around the resultant momentum of the generator-level visible decay products of a hadronically (leptonically) decaying top quark. Here Δy and $\Delta \phi$ represent the differences in rapidities and azimuthal angles of the two objects in consideration. The fatjets have been cleaned using the soft-drop procedure [20] with $\beta=0$ and $z_{\rm cut}=0.1$, which is one of the standard configurations used at the CMS experiment [21]. The aforementioned jet clustering and cleaning have performed using FastJet v3.2.1 [19].

Jet images are preprocessed with certain transformations to aid the network in learning their features, so as to improve the classification performance. The preprocessing procedure follows the methodology described in Ref. [22]. In this technique, the momentum of a jet is rescaled such that its new mass has a fixed value m_B , and boosted to a frame where its energy is has a constant value E_B . Consequently, the boost factor $\gamma_B = E_B/m_B$ assumes a fixed value irrespective of the initial momentum of the jet. One advantage of this preprocessing is that the transformed jets are neither too heavily boosted nor not boosted at all, since either scenario is not expected to well suited for image based classification. It is to be noted that the ratio γ_B is the physical parameter of

import, and not the individual values of m_B and E_B . In this study, we set $\gamma_B=2$, ensuring the subjets are well resolved. A Gram-Schmidt transformation is applied to the jet such that the image plane is perpendicular to the jet axis. The image of a jet is a 50×50 histogram which is filled with the fraction of the jet's energy carried by each its components.

Fig. 1 shows the images of preprocessed leptonic hadronic top (from the $t\bar{t}$ sample) and light flavor QCD jets. In general, a brighter spot mainly due to the leading subjet is observed, along with a less sharp spot surrounded by a diffuse cloud due to the subleading subjets. For the $t\bar{t}$ hadronic case (left), the spread is more closer to the second spot where as for QCD (right), it is more diffused. It can be attributed to the fact that the three subjets inside the top jet correspond to three genuine partons, where as for QCD, subjets are expected to be contaminated by soft radiation. For the leptonic top, comparatively two well separated spots are observed (middle), which are mainly due to the b-like and a subjet with lepton inside, surrounded by a spread due to the third subjet. Note that in the absence of any color connection between the b quark and leptons, spread is not seen between leading and sub-leading subjets like the image for hadronic top. The NN is able to distinguish between different categories of jet images by learning these distinct features. It is to be noted that we separate each jet into its track, photon, and neutral hadron components, and thus three images for each jet (i.e. three input channels) are used to train the network. The network architecture used in this study is described in Fig. 2. The hyperparameters (like the number of channels, kernel sizes, number of nodes, etc.) have been slightly adjusted in order to obtain a reasonably good compromise between the performance and training time. For the purpose of training the network, we have used the Xavier initialization [23] for the weights and the Adam gradient descent [24] with a batch size of 100 and a learning rate (step size of the gradient descent) of 0.001. We have implemented the aforementioned architecture using the gluon API of Apache MXNet v1.5.1 [25] in python.

TOP TAGGING: Network trainings are performed using about 1.2M images for each of the signal and background processes for three sets: (i) hadronic top and QCD jets, (ii) leptonic top and QCD jets, and (iii) leptonic and hadronic top jets. Approximately 135K/135K signal/background jet images are used for the purpose of testing to ensure that the network is not overtrained. The network is trained for 25 epochs, where the training and testing losses are found to saturate to almost identical values. Fig. 3 shows the Receiver Operating Characteristics (ROC) curves to illustrate the hadronic/leptonic top against QCD jet discrimination in solid red/blue (left). Clearly, leptonic top jets are better tagged than hadronic ones. This can be attributed to the comparatively clean environment of the leptonic decay mode, which is evident in the jet images presented in Fig.1. The robustness of the CNN trainings are tested on top jets from the

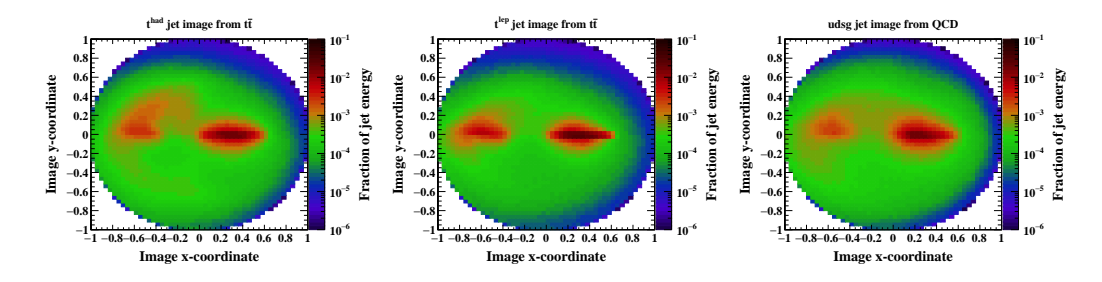


FIG. 1. Images of hadronic (left) and leptonic (middle) top jets from $t\bar{t}$ events, and light flavor QCD jets (right). These are the inclusive images of jets where the track, photon and neutral hadron components have been combined.

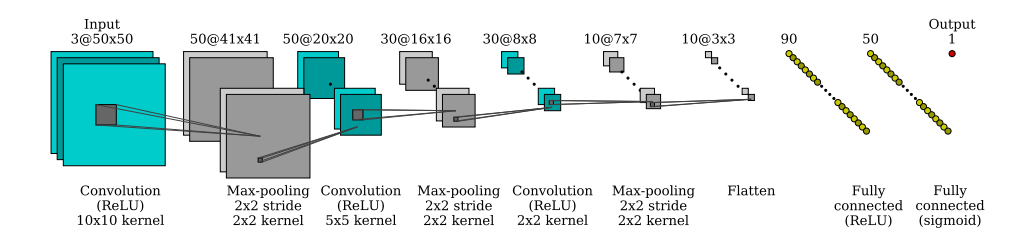


FIG. 2. A schematic diagram of the network structure. For any given layer, the text above it indicates the shape of the layer. The shape of a convolution/max-pooling layer (in cyan/gray squares) is represented as channels $@N \times N$. For a fully-connected layer (in yellow circles) it's a single number corresponding to its number of nodes. The text at the bottom indicates the details of the operation performed on the layer above it in order to obtain the next layer. This includes the kernel sizes used for the convolution and the max-pooling operations, along with the activation function (ReLU/sigmoid). This diagram has been generated by adapting the code from https://github.com/gwding/draw_convnet.

aforementioned W' samples, and the corresponding performances are presented by dashed lines in Fig. 3 (left). The differences between the ROC curves for $t\bar{t}$ and W' samples are primarily due to higher p_T of top jets originating from massive W'. However, we have checked that without the jet preprocessing discussed in the previous section, the observed differences are far more significant. Further, the robustness of the leptonic top tagging is also examined by training the CNN with hadronic top jets from $t\bar{t}$ as background, and the corresponding performances are presented in Fig.3(right) by solid lines testing on $t\bar{t}$ (red) and W'(blue) samples. The difference in performance between the two samples is small.

We try to improve the obtained tagging performances for both hadronic and leptoni channel further by training a Boosted Decision Tree (BDT) on $t\bar{t}$ sample, implemented in TMVA [26] framework. In this training, apart from CNN classifier, the additional variables used are, (i) mass of the jet (m_j) , (ii) the ratios of N-subjettiness variables such as, τ_2/τ_1 , τ_3/τ_2 and τ_4/τ_3 [27]. Here τ_N is defined as, $\tau_N = (R_0 \sum_k p_{T,k})^{-1} \sum_k p_{T,k} \min(\Delta R_{1,k}, R_{2,k}, ... R_{N,k})$,

 $\Delta R_{i,k}$ are the geometrical separations between *i*-th subjet and *k*-th subjettiness axes, and R_0 is the jet radius. The BDT based performances (labeled CNN+BDT) are presented along with the CNN performances in Fig.3. Even in this case also the robustness of the training is verified by evaluating the BDT on top jets from top and W' events. An overall improvement over the CNN train-

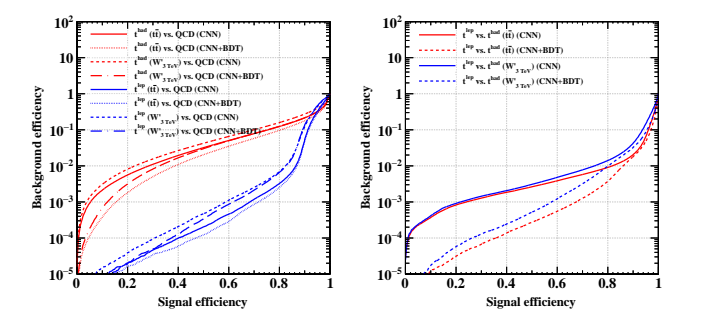


FIG. 3. The ROC curves (left) corresponding to the hadronic (leptonic) top versus QCD jet trainings in red (blue). The leptonic top tagging ROC (right) using hadronic top jets as the background.

ing is observed. For instance, the discrimination against QCD jets, the CNN+BDT performance is better by a factor of $\approx 1.5\text{-}2$ at 40% signal efficiency. On the other hand, the leptonic versus hadronic top jet discrimination improves almost by a factor of ≈ 10 at the same signal efficiency.

TOP POLARIZATION: In this section we study the measurement of boosted top quark polarization using jet images, and then compare the performance with the typical kinematic polarimeter variables [6, 9]. Recall, that the angular distributions of top quark decay products are governed by the structure of its coupling [28]. It is worth noting here, in case of hadronic decaying top

quark, the d-type quark from W decay carries the maximum spin analyzing power, i.e strongly correlated with the top quark spin [28]. Consequently, in case of right handed hadronic decaying top quark, the d-type quark is expected to be more boosted compared to the b and u quarks which are not so boosted, and hence widely separated. On contrary, the b and u quarks are more boosted, and thus less separated in case of left handed hadronic top [6]. For leptonically decaying top quark. the lepton (b quark) is more boosted compared to the bquark (lepton) for right (left) handed top quark. Thus one can expect these features of top quark decay products to construct various polarization observables [3–6]. These polarization driven kinematic features also manifest themselves in the corresponding jet images, which can thereby be exploited to train CNN to learn about the effect of polarization of boosted top quark.

Following the same methodology as described before, preprocessed jet images of top jets are produced from SUSY sample where polarization of top quark is set to either left or right handed. Fig. 4, presents the jet images (component inclusive) for left (upper left) and right (upper right) handed hadronic top quark. The corresponding track component images are also shown in the lower panel of the same figure. The subtle differences between the images corresponding to left and right handed top quark can be understood following the above arguments explaining the correlation of momenta of decay products with its spin. Those suggest that for right handed hadronically decaying boosted top jets, the left (weaker) spot is more diffused and connected to the right (harder) ones, compared to the image corresponding to left handed top jets. This can be attributed to the fact that the right brighter spot is often formed by the leading d (b or u) like subjet, while comparatively less brighter left spot is due to the b + u (u + d or b + d) system for right (left) polarized top quark. Hence, for right handed top jet two spots are more connected as the u and d quark-like jets are strongly color connected among themselves, whereas for left handed case, brighter spot is formed by a boosted leading subjet. Almost similar patterns are observed for the images constructed out of the corresponding tracks, where two clear spots are observed with comparatively less spread due to the absence of much hadronic activities around them. Fig. 5 presents the preprocessed jet images for left (upper left) and right (upper right) polarized leptonic top jets. The middle and lower panels show the images corresponding to track and neutral hadron components respectively. Notably, significant differences in jet images are observed for the two states of polarization of top quark. It is to be noted here, that the charged lepton plays the same role as the d-quark of hadronic top, and hence the same arguments as discussed above can be applied here also in order to understand the pattern of jet images. Accordingly, the brighter right spot is more often formed by the lepton (b quark) for right (left) handed top jets. Thus the track component of this spot is harder for the right handed case, whereas the neutral

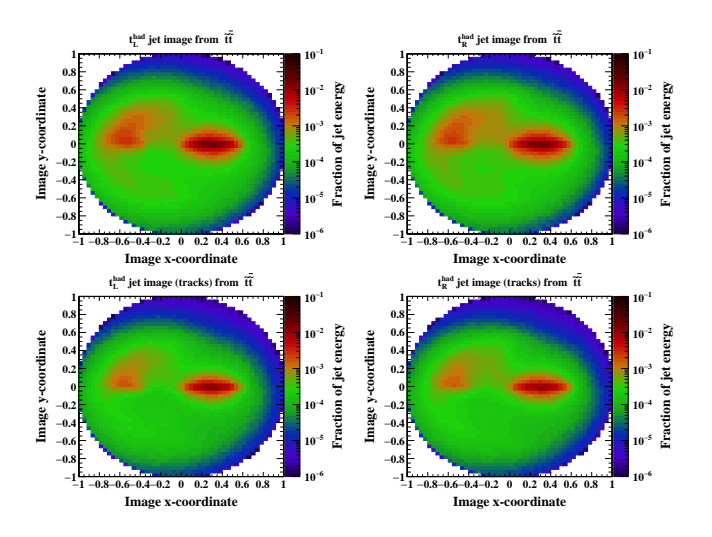


FIG. 4. The top row presents the images of left-handed (left) and right-handed (right) hadronic top jets from \tilde{t}_1 -pair events. The corresponding track component images are shown in the lower row.

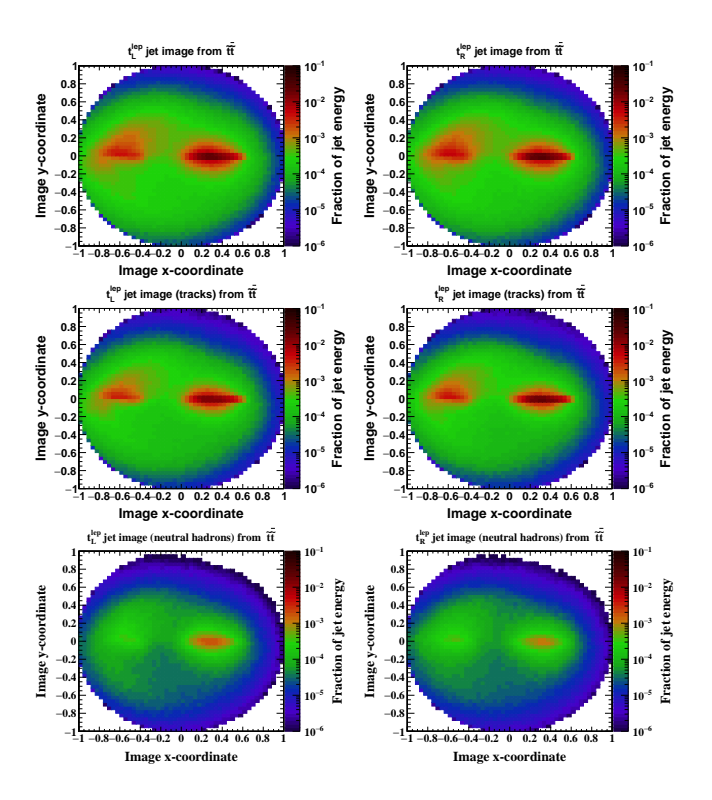


FIG. 5. The top row presents the images of left-handed (left) and right-handed (right) leptonic top jets from \tilde{t}_1 -pair events. The corresponding track (neutral hadron) component images are shown in the middle (lower) row.

hadron component is softer. The CNN is trained (tested) using about 1M/1M (115K/115K) left/right handed top jet images from the SUSY sample. This training is also evaluated on W^\prime sample to validate its robustness.

A robust angular variable, namely $\cos\theta^{\star}$, is constructed out of the momenta of subjets inside the top

jet. This has been proposed to be a powerful discriminator for distinguishing between left and right handed top quarks [6]. As stated before, the d quark has the maximum spin analyzing power in a hadronic top quark decay. Hence, in this methodology, the challenge is to identify of d-like subjet. Currently, techniques are available using ML tools to tag b-jets inside the boosted top jet [29], and can be used as a handle to find the boosted d-like subjet. However, it is beyond the scope of the present analysis to implement such technique. We follow the procedure described in [6], where two subjets whose invariant mass closest to the W boson mass are labeled as non-b subjets. and the third subjet is labeled as b-like. Then comparing invariant masses between the b-like subjet and the other other two subjets (say, j_1 and j_2) the d-like subjet is identified. For instance, if $m_{bj_1} < m_{bj_2}$, then j_1 is identified as the d-like subjet and used to construct $\cos \theta^*$ as,

$$\cos \theta^* = \frac{\vec{j}_t \cdot \vec{j}_d'}{|\vec{j}_t||\vec{j}_d'|}.$$
 (1)

Here \vec{j}_t is the momentum of reconstructed top jet in the lab frame, and \vec{j}'_d is the momentum of the d-like subjet $(j_1 \equiv j_d)$ in the top rest frame. For the leptonic case, lepton energy fraction $z_{\ell} = E_{\ell}/E_t$ acts as a sensitive polarimeter [9]. Here E_{ℓ} and E_{t} are the energies of the lepton track and the top jet respectively, in the lab frame. We use the following procedure to ensure lepton track isolation. The top jet constituents are exclusively clustered into two k_T subjets. The mini-isolation [30], value is computed for the leading (highest p_T) track inside each subjet. The track with smaller mini-isolation is identified as the lepton track. It is found that about 80% cases this track matches with the MC truth level lepton. The ROC curves corresponding to $\cos \theta^*$ (dashed lines) and the CNN classifier (solid lines) are presented in Fig. 6 (left), for left and right handed hadronic top jets from SUSY sample (in red). The performance of the CNN training when evaluated on top jets from the W' sample is also shown (in blue). The analogous ROC curves for the leptonic top jets are presented in the right plot of the same figure. Evidently, the CNN classifiers outperform the kinematic variables, for both leptonic and hadronic top jets. Impact of polarization sensitive variables is estimated measuring a physical quantity, namely asymmetry, as defined.

$$A_v^P = \frac{N_{v>c} - N_{vc} + N_{v$$

Here $N_{v>c}$ is the number of top jets subject to the condition that its polarization discriminator $v \ (\equiv \cos \theta^*, z_\ell, or CNN \ classifier)$ is greater than a given threshold c, and $N_{v<c}$ is defined similarly. The superscript P refers to the polarization composition of the top jets in a given sample. Recall that we consider only the two extreme compositions (entirely left or right handed) in this study. The magnitude of the difference $D_v = |A_v^L - A_v^R|$ is a measure of the sensitivity of v to the top quark polarization. Needless to say, this difference will be very small if v

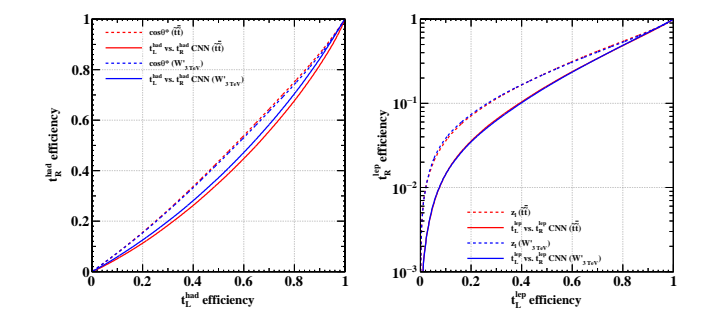


FIG. 6. The left plot shows the discrimination (ROC curve) between left-handed and right-handed hadronic top jets using $\cos \theta^*$ (dashed) and the CNN classifier (solid) in \tilde{t}_1 -pair (red) as well as W' (blue) events. Note that the CNN trained on top jets from \tilde{t}_1 -pair events has been evaluated on top jets from W' events. The right plot shows the same for leptonic top jets, except that the z_ℓ variable is used instead of $\cos \theta^*$.

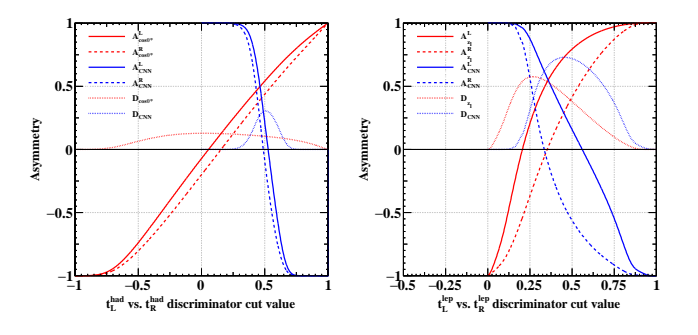


FIG. 7. The asymmetry variables (Eq. 2) and their absolute differences between the left and right polarized cases are shown as a function of the discriminator threshold, corresponding to different polarization discriminators, using hadronic (left) and leptonic (right) top jets from the SUSY sample.

is not very sensitive to polarization. The optimum value of c for a given discriminator v, is the point at which D_v is maximum. Naturally, the most sensitive polarization discriminator is decided by comparing the peak values of D_v . The asymmetries and their differences are presented in Fig. 7 for hadronic (left) and leptonic (right) top jets from the SUSY sample. It is evident from the peak value of D_v , that the CNN classifier is ≈ 2 times more sensitive compared to $\cos\theta^*$ for hadronic top jets, and ≈ 1.3 times more sensitive than z_ℓ for the leptonic case.

Summary: In this letter we study the boosted top tagging performances in its hadronic and leptonic channel using images of jets to train CNN. We demonstrate that the top jet tagging performance can be improved further employing BDT traing using output of CNN classifier along with other high level inputs. Performances of the boosted top tagging using in its leptonic channel using ML tools are also presented. The ROC curves show that the top jet tagging efficiencies for leptonic channel much better in comparison to hadronic channel. Furthermore, with the motivation that the polarization measure-

ment of top quark can reveal the signature of new physics, we explore to improve the performances in identifying and measuring top quark polarization. The results indicate that the CNN classifier is more sensitive to polarization than kinematic polarimeter variables like $\cos\theta^*$ and z_{θ} .

- J. M. Butterworth, A. R. Davison, M. Rubin, and G. P. Salam, Jet substructure as a new Higgs search channel at the LHC, Phys. Rev. Lett. 100, 242001 (2008), arXiv:0802.2470 [hep-ph].
- [2] S. Marzani, G. Soyez, and M. Spannowsky, Looking inside jets: an introduction to jet substructure and boosted-object phenomenology, Vol. 958 (Springer, 2019) arXiv:1901.10342 [hep-ph].
- [3] J. Shelton, Polarized tops from new physics: signals and observables, Phys. Rev. D 79, 014032 (2009), arXiv:0811.0569 [hep-ph].
- [4] D. Krohn, J. Shelton, and L.-T. Wang, Measuring the Polarization of Boosted Hadronic Tops, JHEP 07, 041, arXiv:0909.3855 [hep-ph].
- [5] Y. Kitadono and H.-n. Li, Jet substructures of boosted polarized hadronic top quarks, Phys. Rev. D 93, 054043 (2016), arXiv:1511.08675 [hep-ph].
- [6] R. Godbole, M. Guchait, C. K. Khosa, J. Lahiri, S. Sharma, and A. H. Vijay, Boosted Top quark polarization, Phys. Rev. D 100, 056010 (2019), arXiv:1902.08096 [hep-ph].
- [7] S. Chatterjee, R. Godbole, and T. S. Roy, Jets with electrons from boosted top quarks, JHEP 01, 170, arXiv:1909.11041 [hep-ph].
- [8] U. Husemann, Top-Quark Physics: Status and Prospects, Prog. Part. Nucl. Phys. 95, 48 (2017), arXiv:1704.01356 [hep-ex].
- [9] R. M. Godbole, S. D. Rindani, and R. K. Singh, Lepton distribution as a probe of new physics in production and decay of the t quark and its polarization, JHEP 12, 021, arXiv:hep-ph/0605100.
- [10] A. J. Larkoski, I. Moult, and B. Nachman, Jet Substructure at the Large Hadron Collider: A Review of Recent Advances in Theory and Machine Learning, Phys. Rept. 841, 1 (2020), arXiv:1709.04464 [hep-ph].
- [11] J. Cogan, M. Kagan, E. Strauss, and A. Schwarztman, Jet-Images: Computer Vision Inspired Techniques for Jet Tagging, JHEP 02, 118, arXiv:1407.5675 [hep-ph].
- [12] A. Butter et al., The Machine Learning Landscape of Top Taggers, SciPost Phys. 7, 014 (2019), arXiv:1902.09914 [hep-ph].
- [13] Z. Sullivan, Fully Differential W' Production and Decay at Next-to-Leading Order in QCD, Phys. Rev. D 66, 075011 (2002), arXiv:hep-ph/0207290.
- [14] T. Sjöstrand, S. Ask, J. R. Christiansen, R. Corke, N. Desai, P. Ilten, S. Mrenna, S. Prestel, C. O. Rasmussen, and P. Z. Skands, An introduction to PYTHIA 8.2, Comput. Phys. Commun. 191, 159 (2015), arXiv:1410.3012 [hep-ph].
- [15] B. Fuks and R. Ruiz, A comprehensive framework for studying W' and Z' bosons at hadron colliders with automated jet veto resummation, JHEP **05**, 032, arXiv:1701.05263 [hep-ph].

- [16] J. Alwall, R. Frederix, S. Frixione, V. Hirschi, F. Maltoni, O. Mattelaer, H. S. Shao, T. Stelzer, P. Torrielli, and M. Zaro, The automated computation of tree-level and next-to-leading order differential cross sections, and their matching to parton shower simulations, JHEP 07, 079, arXiv:1405.0301 [hep-ph].
- [17] J. de Favereau, C. Delaere, P. Demin, A. Giammanco, V. Lemaître, A. Mertens, and M. Selvaggi (DELPHES 3), DELPHES 3, A modular framework for fast simulation of a generic collider experiment, JHEP 02, 057, arXiv:1307.6346 [hep-ex].
- [18] M. Cacciari, G. P. Salam, and G. Soyez, The anti- k_T jet clustering algorithm, JHEP **04**, 063, arXiv:0802.1189 [hep-ex].
- [19] M. Cacciari, G. P. Salam, and G. Soyez, FastJet user manual, Eur. Phys. J. C 72, 1896 (2012), arXiv:1111.6097 [hep-ph].
- [20] A. J. Larkoski, S. Marzani, G. Soyez, and J. Thaler, Soft Drop, JHEP 05, 146, arXiv:1402.2657 [hep-ph].
- [21] A. M. Sirunyan et al. (CMS), Identification of heavy, energetic, hadronically decaying particles using machine-learning techniques, JINST 15 (06), P06005, arXiv:2004.08262 [hep-ex].
- [22] T. S. Roy and A. H. Vijay, A robust anomaly finder based on autoencoders (2019), arXiv:1903.02032 [hep-ph].
- [23] X. Glorot and Y. Bengio, Understanding the difficulty of training deep feedforward neural networks, in Proceedings of the Thirteenth International Conference on Artificial Intelligence and Statistics, Proceedings of Machine Learning Research, Vol. 9, edited by Y. W. Teh and M. Titterington (PMLR, Chia Laguna Resort, Sardinia, Italy, 2010) pp. 249–256.
- [24] D. P. Kingma and J. Ba, Adam: A method for stochastic optimization (2014), arXiv:1412.6980 [cs.LG].
- [25] T. Chen, M. Li, Y. Li, M. Lin, N. Wang, M. Wang, T. Xiao, B. Xu, C. Zhang, and Z. Zhang, Mxnet: A flexible and efficient machine learning library for heterogeneous distributed systems, CoRR abs/1512.01274 (2015), arXiv:1512.01274.
- [26] A. Hocker et al., TMVA Toolkit for Multivariate Data Analysis (2007), arXiv:physics/0703039.
- [27] J. Thaler and K. Van Tilburg, Identifying Boosted Objects with N-subjettiness, JHEP 03, 015, arXiv:1011.2268 [hep-ph].
- [28] M. Jezabek and J. H. Kuhn, Lepton Spectra from Heavy Quark Decay, Nucl. Phys. B 320, 20 (1989).
- [29] A. Sirunyan et al. (CMS), Identification of heavy-flavour jets with the CMS detector in pp collisions at 13 TeV, JINST 13 (05), P05011, arXiv:1712.07158 [physics.insdet].
- [30] V. Khachatryan *et al.* (CMS), Search for supersymmetry in pp collisions at $\sqrt{s} = 13$ TeV in the single-lepton final state using the sum of masses of large-radius jets, JHEP **08**, 122, arXiv:1605.04608 [hep-ex].